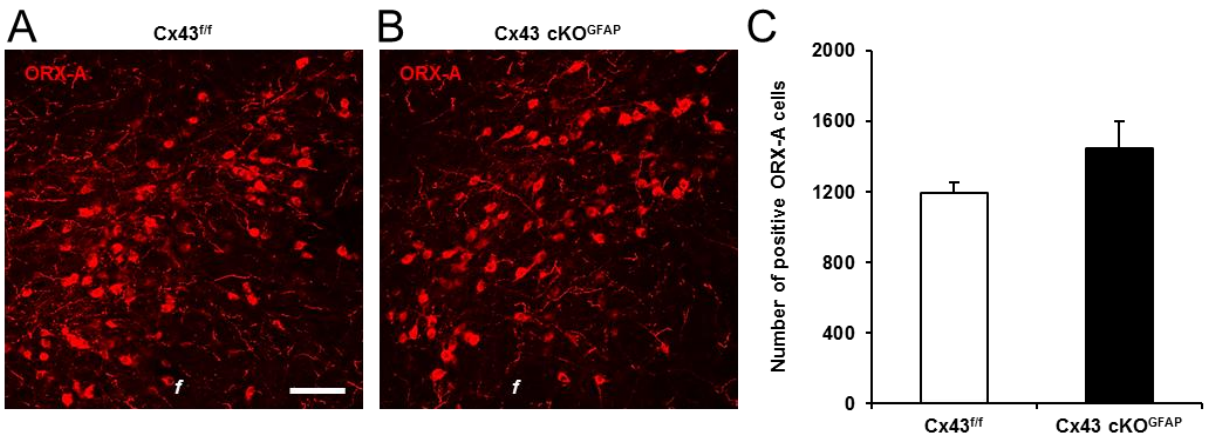

Supplemental Figure S1. Orexin-A immunoreactivity in the lateral hypothalamic area of Cx43$^{f/f}$ and Cx43 cKO^{GFAP} mice, related to Figure 1. (A and B) Representative sections of the lateral hypothalamic area (LHA) from Cx43$^{f/f}$ (A) and Cx43 cKO^{GFAP} mice (B) stained with an antibody directed against orexin (ORX)-A. f: fornix. Scale bar: 100 µm. (C) Average number of ORX-A positive cells in the LHA of Cx43$^{f/f}$ and Cx43 cKO^{GFAP} mice. No differences were observed between Cx43$^{f/f}$ (n=4) and Cx43 cKO^{GFAP} mice (n=3; Student t-test, $p>0.05$).

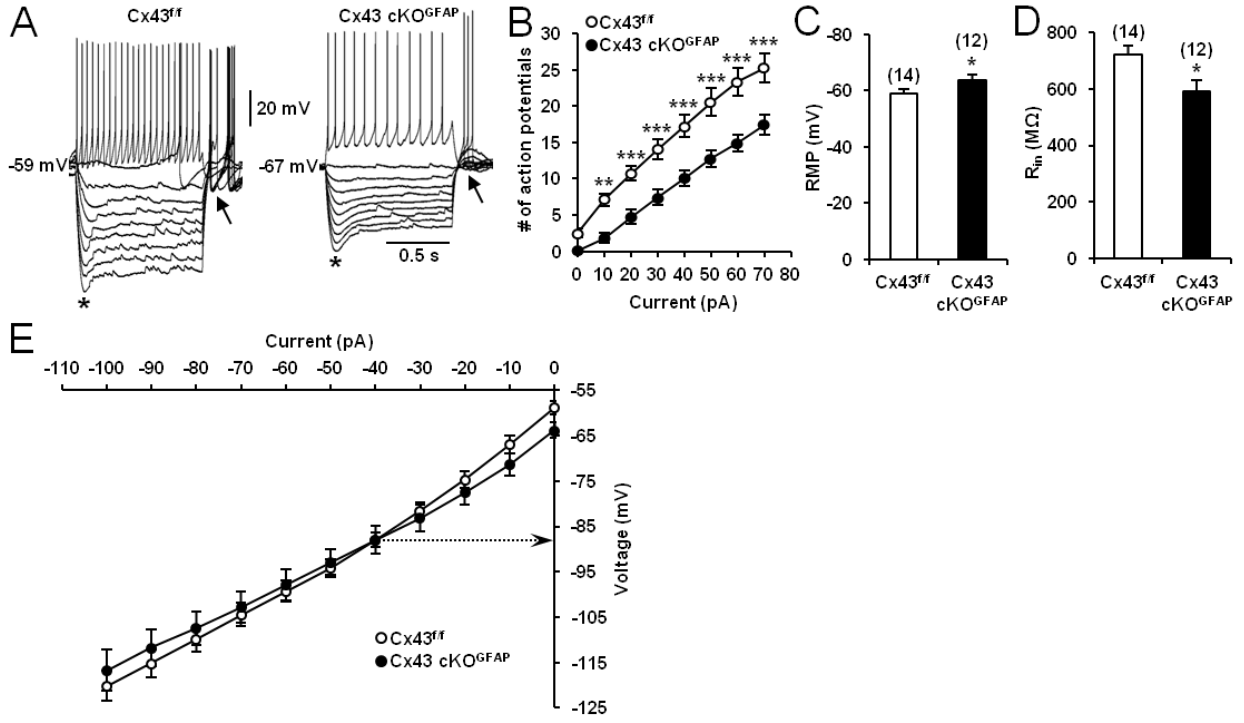

Supplemental Figure S2. Electrical membrane properties of orexin neurons from Cx43$^{f/f}$ and Cx43 cKO^{GFAP} mice, related to Figure 2. (A) Responses of two orexin neurons from Cx43$^{f/f}$ (left) and Cx43 cKO^{GFAP} mice (right) to current pulses from –80 pA to 70 pA (1 s, 10 pA increments). For more clarity during depolarizing pulses, only the response to the current injection of 50 pA is shown. Asterisks and arrows indicate an I_h current and a low-threshold spike, respectively, in response to hyperpolarizing currents. (B) Summary of current-firing curves in orexin neurons from Cx43$^{f/f}$ (n=14 cells from 9 animals) and Cx43 cKO^{GFAP} mice (n=12 cells from 6 animals; ANOVA followed by post-hoc test, **p<0.01 and ***p<0.001). (C) Average resting membrane potential (RMP) of orexin neurons from Cx43$^{f/f}$ (n=14 cells from 9 animals) and Cx43 cKO^{GFAP} mice (n=12 cells from 6 animals; Student t-test, *p<0.05). (D) Average input resistance (R_{in}) of orexin neurons from Cx43$^{f/f}$ (n=14 cells from 9 animals) and Cx43 cKO^{GFAP} mice (n=12 cells from 6 animals; Student t-test, *p<0.05). (E) Average current-voltage relationships in orexin neurons recorded from Cx43$^{f/f}$ (n=14 cells from 9 animals) and Cx43 cKO^{GFAP} mice (n=12 cells from 6 animals). Note that the two curves converge at a voltage of – 88 mV (dotted arrow).

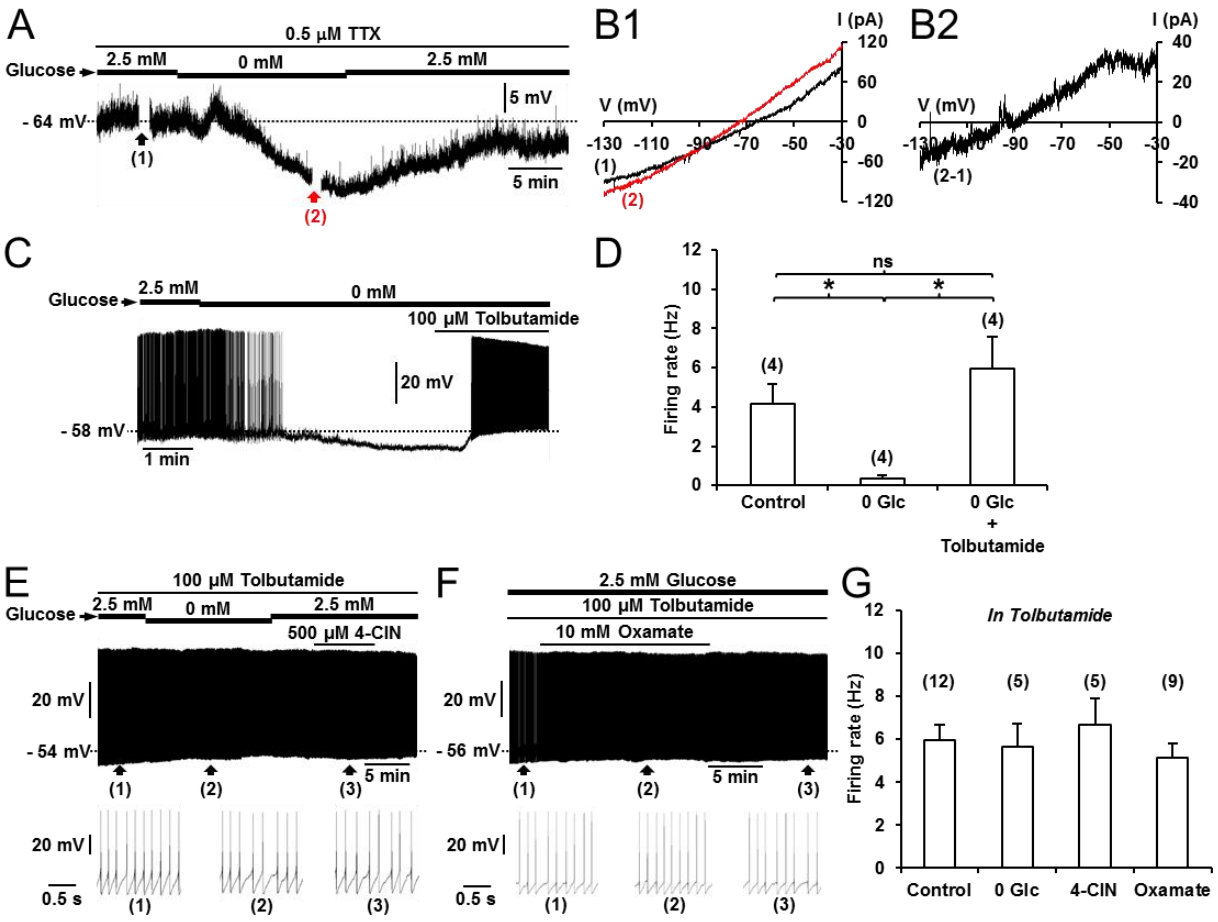

Supplemental Figure S3. Inhibition of orexin neurons from Cx43$^{f/f}$ mice induced by lactate shortage is mediated by K_{ATP} channels, related to Figure 3. (A) Whole-cell current-clamp recording of an orexin neuron from Cx43$^{f/f}$ mouse showing that glucose deprivation evoked a membrane hyperpolarization in the presence of tetrodotoxin (TTX). Arrows indicate the time of application of voltage ramps before (1) and during (2) glucose deprivation to trace the current-voltage relationship. (B1 and B2) Current traces evoked by the voltage ramps (5 s) applied in (A) from –130 mV to –30 mV at a holding potential of –64 mV. (B1) Current responses to the voltage ramp before (1) and during (2) glucose deprivation. (B2) Glucose deprivation-induced current obtained after subtracting the current response to voltage ramps in the baseline condition (1) from that during glucose deprivation (2). (C) Whole-cell current-clamp recording of an orexin neuron from Cx43$^{f/f}$ mouse showing that bath application of the K_{ATP} channel blocker, tolbutamide, induced membrane depolarization and restored tonic spike firing during glucose deprivation. (D) Average firing frequency of orexin neurons from Cx43$^{f/f}$ mice exposed to different conditions (in 2.5 mM glucose (Control); in 0 mM glucose (0 Glc); in 0 mM glucose with tolbutamide; n=4 cells from 4 animals for each condition; ANOVA followed by post-hoc test, *p<0.05; ns, nonsignificant). (E and F) Whole-cell current-clamp recordings of two orexin neurons from Cx43$^{f/f}$ mice showing that bath application of tolbutamide (>15 min) prevented the inhibitory effect of glucose deprivation and 4-CIN (E), and oxamate (F). (G) Average firing frequency of orexin neurons from Cx43$^{f/f}$ mice exposed to different conditions during tolbutamide treatment (with 2.5 mM glucose (Control), n=12 cells from 7 animals; with 0 mM glucose (0 Glc); n=5 cells from 5 animals; with 4-CIN, n=5 cells from 4 animals; with oxamate, n=9 cells from 4 animals; ANOVA followed by post-hoc test, p>0.05).

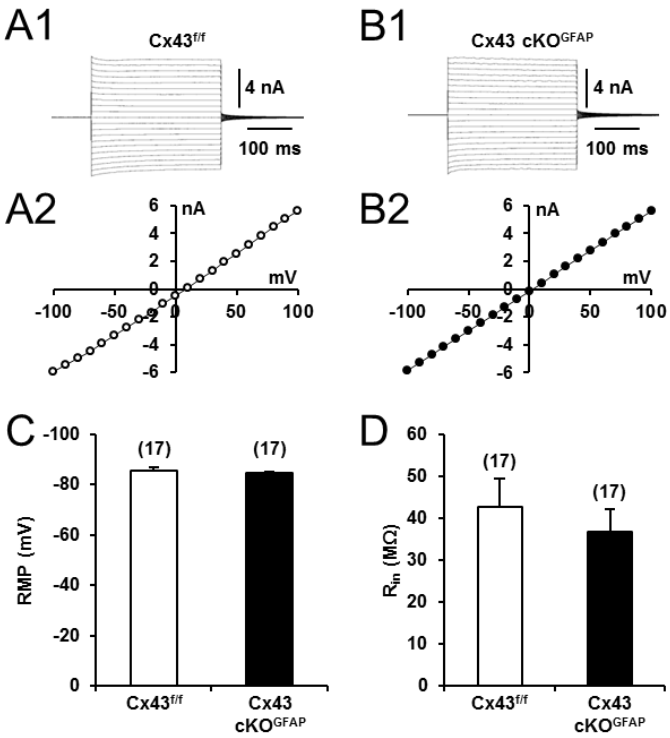

Supplemental Figure S4. Passive electrophysiological membrane properties of LHA astrocytes from Cx43$^{f/f}$ and Cx43 cKO^{GFAP} mice, related to Figure 5. (A1) Whole-cell current of an astrocyte recorded in the LHA of Cx43$^{f/f}$ mouse in response to a series of 300 ms voltage pulses from –100 mV to +100 mV with 10 mV increasing voltage steps applied at a holding potential of –80 mV. (A2) Current-voltage relationship from the astrocyte recorded in (A1). (B1 and B2) Same experiments as in (A1) and (A2) but performed in Cx43 cKO^{GFAP} mouse. (C and D) Average resting membrane potential (RMP, C) and input membrane resistance (R_{in}, D) of LHA astrocytes in Cx43$^{f/f}$ (n=17 cells from 5 animals) and Cx43 cKO^{GFAP} mice (n=17 cells from 3 animals; Student t-test, p>0.05).

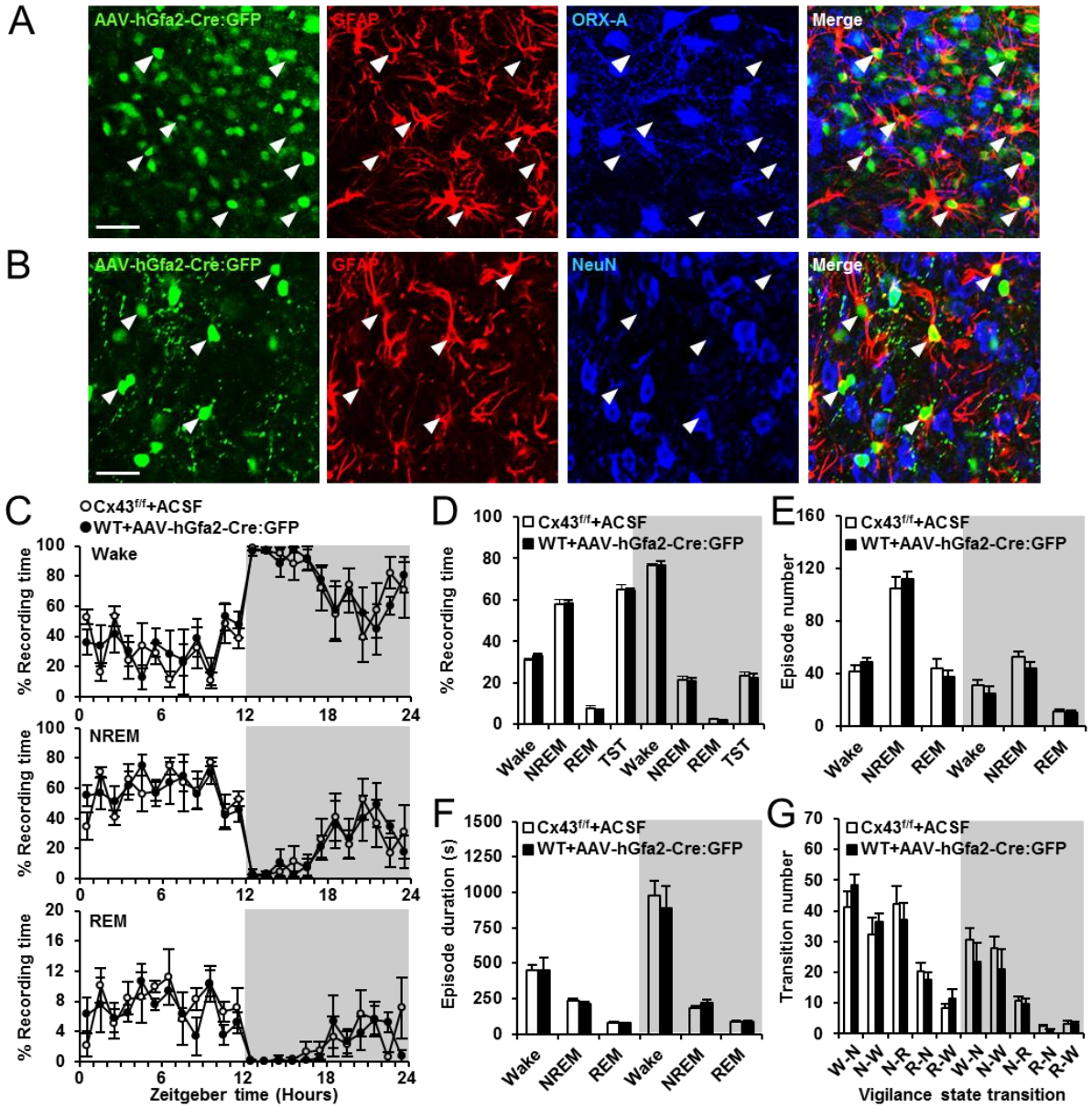

Supplemental Figure S5. Injection of AAV-hGfa2-Cre:GFP in the LHA selectively targets astrocytes, related to Figure 7. (A) Sections of the LHA from Cx43$^{f/f}$ mouse double stained with antibodies against GFAP and orexin (ORX)-A 21 days after injection of AAV-hGfa2-Cre:GFP into the LHA. Cre:GFP-expressing cells (green, arrowheads) were positive for GFAP (red) but not for ORX-A (blue). Note that Cre:GFP expression was nuclear. (B) Same as in (A), but with NeuN antibody instead of ORX-A. Cre:GFP-expressing cells (green, arrowheads) were positive for GFAP (red) but not for NeuN (blue). Scale bars (A, B): 40 µm. (C-G) Sleep-wake parameters in two control groups of animals: (i) Wild-type (WT) mice injected with AAV-hGfa2-Cre:GFP into the LHA (WT+AAV-hGfa2-Cre:GFP, n=4) and (ii) Cx43$^{f/f}$ mice injected with ACSF into the same brain region (Cx43$^{f/f}$+ACSF, n=4) measured 21 days after injection. (C and D) Percentage average of time spent in wake, NREM and REM sleep per hour (C; ANOVA, $p>0.05$) and over 12h (D; ANOVA, $p>0.05$). (E-G) Average number (E) and duration (F) of wake, NREM and REM sleep episodes and transition number between all vigilance states (G) during the light and dark phases in both groups (ANOVA, $p>0.05$ for E-G).